Eur J Vasc Endovasc Surg (2016) 51, 44–55

An Experimental Evaluation of Device/Arterial Wall Compliance Mismatch for Four Stent-Graft Devices and a Multi-layer Flow Modulator Device for the Treatment of Abdominal Aortic Aneurysms

L. Morris [a], **F. Stefanov** [a], **N. Hynes** [b], **E.B. Diethrich** [c], **S. Sultan** [b,d,*]

[a] Galway Medical Technologies Centre (GMedTech), Department of Mechanical and Industrial Engineering, Galway Mayo Institute of Technology, Galway, Ireland
[b] Galway Clinic, Royal College of Surgeons of Ireland Affiliated Hospital, Doughiska, Galway, Ireland
[c] Cardiovascular and Thoracic Surgery, Arizona Heart Foundation, Phoenix, AZ, USA
[d] Western Vascular Institute, Department of Vascular and Endovascular Surgery, University Hospital Galway, National University of Ireland, Galway, Ireland

WHAT THIS PAPER ADDS

Loss of arterial compliance is an important cardiovascular risk factor. Compliance decreases with age, hypertension, and menopause, and its reduction is associated with endothelial dysfunction and adverse cardiovascular events. Pathological loss of compliance is, usually, an insidious process. However, endograft placement results in a more acute drop in compliance, which not only effects cardiovascular risk, but, also, through the fluid structure interactions may influence stent graft durability and the development of complications. The variation in compliance between commercially available stent grafts was investigated to examine which devices have the least adverse effect on aortic compliance.

Objective/background: To investigate experimentally the arterial wall/device compliance mismatch of four stent-graft devices and a multilayer flow modulator within the supra- and infrarenal locations for the treatment of abdominal aortic aneurysms (AAA).

Methods: Five devices (MFM, EndurantII, Excluder, Zenith, and Fortron) were tested under physiological flow conditions within a flow simulator system comprising of a patient-specific thin-walled flexible AAA perfusion model with replicated intraluminal thrombus, supported by the spinal column. Devices were submitted to circumferential force tests and implanted in the perfusion model for circumferential arterial pressure/diameter measurements. Parameters, including radial resistive force, supra-/infrarenal compliance, pulsatile arterial energy loss (PAEL), pulse wave velocity (PWV), and wave reflection coefficient (Γ), were computed to characterise the devices' performance.

Results: The Zenith and EndurantII devices had the highest radial resistive force (up to 3 N/cm), while the Fortron device had the lowest (0.11 N/cm). Supra- and infrarenal compliance varied between 6.9–5.1 $\times$ 10^{-4}/mmHg and 4.8–5.4 $\times$ 10^{-4}/mmHg, respectively. Two devices (EndurantII and Excluder) significantly decreased infrarenal compliance by 13–26% ($p < .001$). Four devices increased the PAEL by 13–44% ($p < .006$). The PWV ranged from 10.9 m/s (MFM; $p = .164$) to 15.1 m/s (EndurantII; $p < .001$). There was an increase of 8–238% ($p < .001$) in the reflection coefficient for all devices.

Conclusion: Commercially available endovascular devices lower the aortic wall compliance after implantation. The MFM was found to be the most compliant in the suprarenal region, while the Fortron device was the most compliant in the infrarenal region. Choosing the most compliant devices for treating AAAs produces positive gains in the aortic elastic recoil, thus minimising the device related complications.

Article history: Received 11 April 2015, Accepted 29 July 2015, Available online 9 September 2015

Keywords: Abdominal aortic aneurysm, Endovascular aortic repair, Endograft, Multilayer flow modulator, Compliance

* Corresponding author. Department of Vascular & Endovascular Surgery, National University of Ireland, Newcastle Road, Galway, Ireland.
E-mail address: sherif.sultan@hse.ie (S. Sultan).

http://dx.doi.org/10.1016/j.ejvs.2015.07.041

INTRODUCTION

Endovascular aneurysm repair (EVAR) is the contemporary first-line therapy for abdominal aortic aneurysms (AAA), with open repair reserved for those who are unfit for EVAR. EVAR offers clear benefits when compared with open repair,

in terms of less trauma, short hospital stay, reduced mortality, and lower morbidity. However, associated device fixation problems, such as endoleaks, migration, and proximal neck enlargement,[1,2] can affect the long-term success.[3] Radial arterial wall compliance (C) is a change in vessel diameter or cross-sectional area triggered by a change in blood pressure. C, relative pulsatility, and pulsatile diameter are dramatically changed following the arterial device implantation.[4,5] The changes in compliance at the interface stent/arterial wall, represent a result of the device-to-arterial wall mechanical coupling. To date, it is unclear how stents affect the compliance of an artery, as compliance varies from one type of stent to another. One stent type can cause the arterial wall to behave rigidly, while another type may have no effect.[6]

The reduction in C influences the haemodynamics in terms of blood flow patterns and von Mises stress in the wall,[7] as was shown by Ene et al.,[8] who computationally analysed six AAAs under different assumptions, such as static/transient pressures, steady/transient flows, and rigid/compliant walls. Vernhet et al. and Morris et al. showed a significant decrease in compliance when using small stents in small-calibre rabbit arteries and a stent-graft (SG) device within an AAA perfusion model, respectively,[2,7] while Pihkala et al. found that implanted stents in pig aortas did not affect C or alter the pulse wave velocity (PWV).[9] Also, *in vivo* monitoring by intravascular ultrasound within coronary lesions shows a decrease in compliance after the implantation of endovascular scaffolds.[10] Changes in C trigger arterial dysfunction and pathophysiology, which have a key role in vascular biomechanics and homeostasis.[11] Vlachopoulos et al. found that a 1 m/s increase in the PWV generates a 14% increased risk of cardiovascular events, cardiovascular mortality, and all-cause mortality.[12]

It was hypothesised, in this study, that SG devices play a major role in altering the local C after implantation. To test the hypothesis four SGs: EndurantII (Medtronic, Dublin Ireland), Fortron (Cordis, Sommerville, NJ, USA), Zenith (Cook Medical, Bloomington, IN, USA), Excluder (Gore Medical, Putzbrunn, Germany) and one Multilayer Flow Modulator (MFM) device (Cardiatis, Isnes, Belgium) were deployed in an AAA perfusion model.

METHODS

SG and MFM devices

Four bifurcated SG devices and the MFM device were dynamically tested within the AAA perfusion model (Fig. 1A).

All SGs have a thin-walled graft covering the aneurysmal sac region (Fig. 1A), while the MFM has no graft. The MFM device is also bifurcated by stapling at the bottom half by the manufacturer, thus creating two tubular channels in which two smaller MFM stents are fitted as device limbs. Table 1 summarises the devices sizes according to instructions for use (IFU). Based on the infrarenal internal/external neck sizes of the AAA, the clinicians sized the devices according to the manufacturers' IFU. The maximum proximal and distal diameters varied from 28—30 mm and 14—16 mm, respectively. The devices were deployed inside the perfusion model, as shown in Fig. 2(A, B), and outer neck diameters were measured at rest without any pressurisation, as shown in Table 2, in order to ensure that the experiment started at similar levels of neck dilatation.

Circumferential force test rig setup

The chronic outward force (COF) is a measure of the force the stent exerts on the artery as it tries to expand to its nominal diameter during vessel expansion. The radial resistive force (RRF) is a measure of the force the stent exerts, as it resists circumferential compression by constriction of the artery. Both parameters depend on the state of compression. The terms COF and RRF were coined by Duerig et al. to better describe the circumferential forces of self-expanding stents.[13]

COF and RRF were measured with the use of a high-strength, low-friction, 10-mm wide and 0.2-mm thick double-strip material (Tyvek paper with polyester/polyethylene laminated film; DuPont, Wilmington, DE, USA) that was looped around the proximal end of the devices, and threaded through a narrow gap between two rollers of the circumferential force test rig (Fig. 1B), similar to the tests conducted by Duda et al.[14] One end of the strip was attached to a fixed base, while the other end was attached to the clamp of a tensile tester machine (Instron 5544; Instron, High Wycombe, UK), equipped with ±10N static load cell.

The devices were mounted on a horizontal bar support, aligned with the material loop, in order to maintain their position during testing (Fig. 1C). There were 10 samples (cycles) per test, done for each SG, at an extension rate of 190 mm/min. The test was repeated 10 times for each device. All devices were compressed circumferentially, by a maximum of 20% reduction in the circumferential length. The reduction in diameter was given by the following formula:

$$\text{Diameter ratio} = 1 - \frac{Cd}{\pi D} \quad (1)$$

where

Cd is the circumferential displacement, D is the maximum proximal diameter of the device.

To ensure full stent expansion before testing devices were preheated in an oven at 45 °C for 10 min. The test started with the SGs expanded to the maximum proximal diameter state. All devices were crimped to 80% of the initial diameter and then unloaded to the nominal outer diameter, forming a cycle or a hysteresis describing the mechanical behaviour of the materials, as shown in Fig. 3.

Patient-specific AAA perfusion model fabrication

A patient-specific thin-walled flexible AAA perfusion model with intraluminal thrombus (ILT), and the inclusion of renal

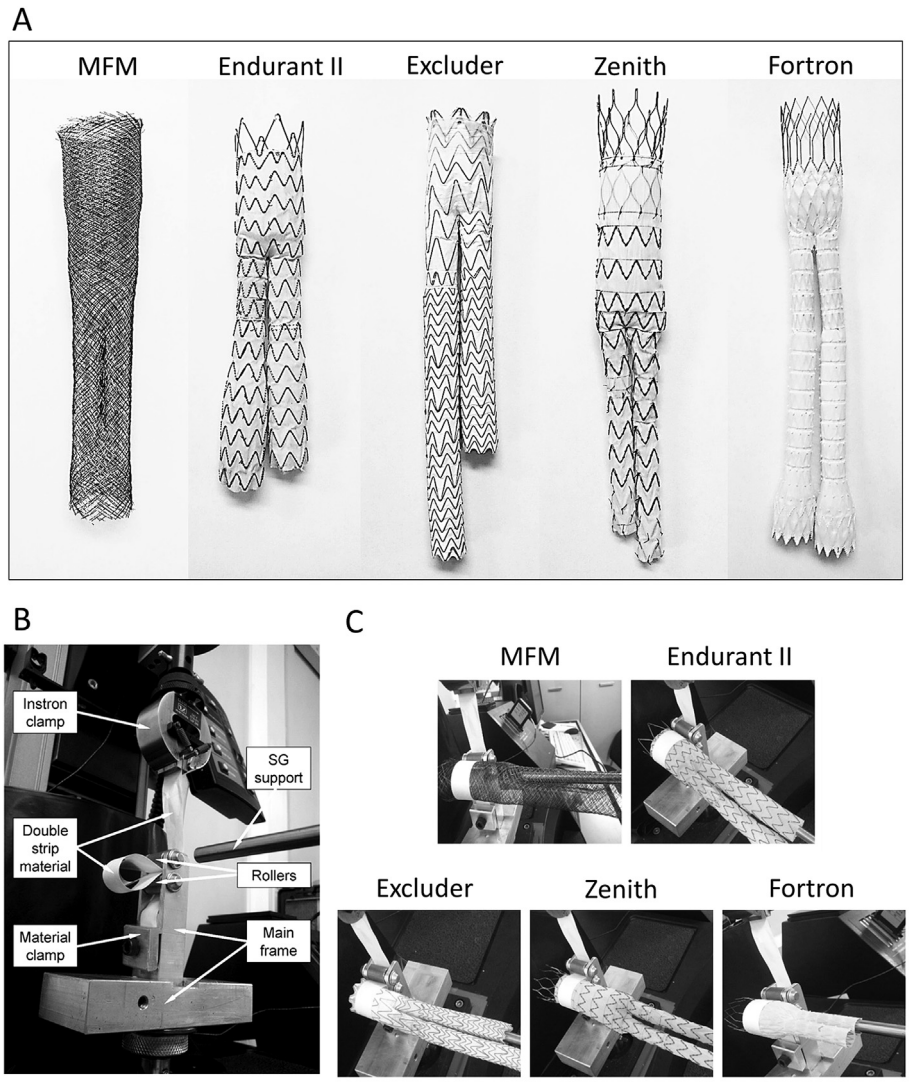

Figure 1. Endovascular devices and circumferential force test rig set-up. (A) Tested commercially available endovascular devices. (B) Test rig for chronic outward and radial resistive circumferential force measurements, mounted on the tensile tester machine (Instron 5544). (C) Endovascular devices mounted on the circumferential force test rig. *Note*. SG = stent-graft.

Table 1. Characteristics of the five endovascular abdominal aortic aneurysm devices.

Device features	MFM	EndurantII	Excluder	Zenith	Fortron
Intended for use aortic vessel diameter (mm)	24–28	23–25	24–26	23–24	23–27
Maximum proximal diameter (mm)	30.0	28.0	28.5	28.0	30.0
Maximum distal diameter (mm)	16.0	16.0	14.5	14.0	16.0
Device length (mm)	150	170	160	184	200
% Degree of oversizing (IFU)	25.0	17.0	18.8	17.0	25.0
Uncovered fixation length (mm)	–	15	0	30	30
Fixation type	Radial force	Radial force, barbs	Radial force, barbs	Radial force, barbs	Radial force, barbs
Proximal fixation location	Suprarenal	Renal	Infrarenal	Suprarenal	Suprarenal
Stent material	Cobalt alloy	Nitinol	Nitinol	Stainless steel	Nitinol
Fabric material	–	Woven polyester	ePTFE	Woven polyester	Woven polyester
Measured wall thickness (mm)	0.7	0.5	0.4	0.4	0.5
Activation type	Self-expanding	Self-expanding	Self-expanding	Self-expanding	Self-expanding
Activation temperature (°C)	–	>30	>30	–	>30

Note. IFU = instructions for use; ePTFE = expanded polytetrafluoroethylene.

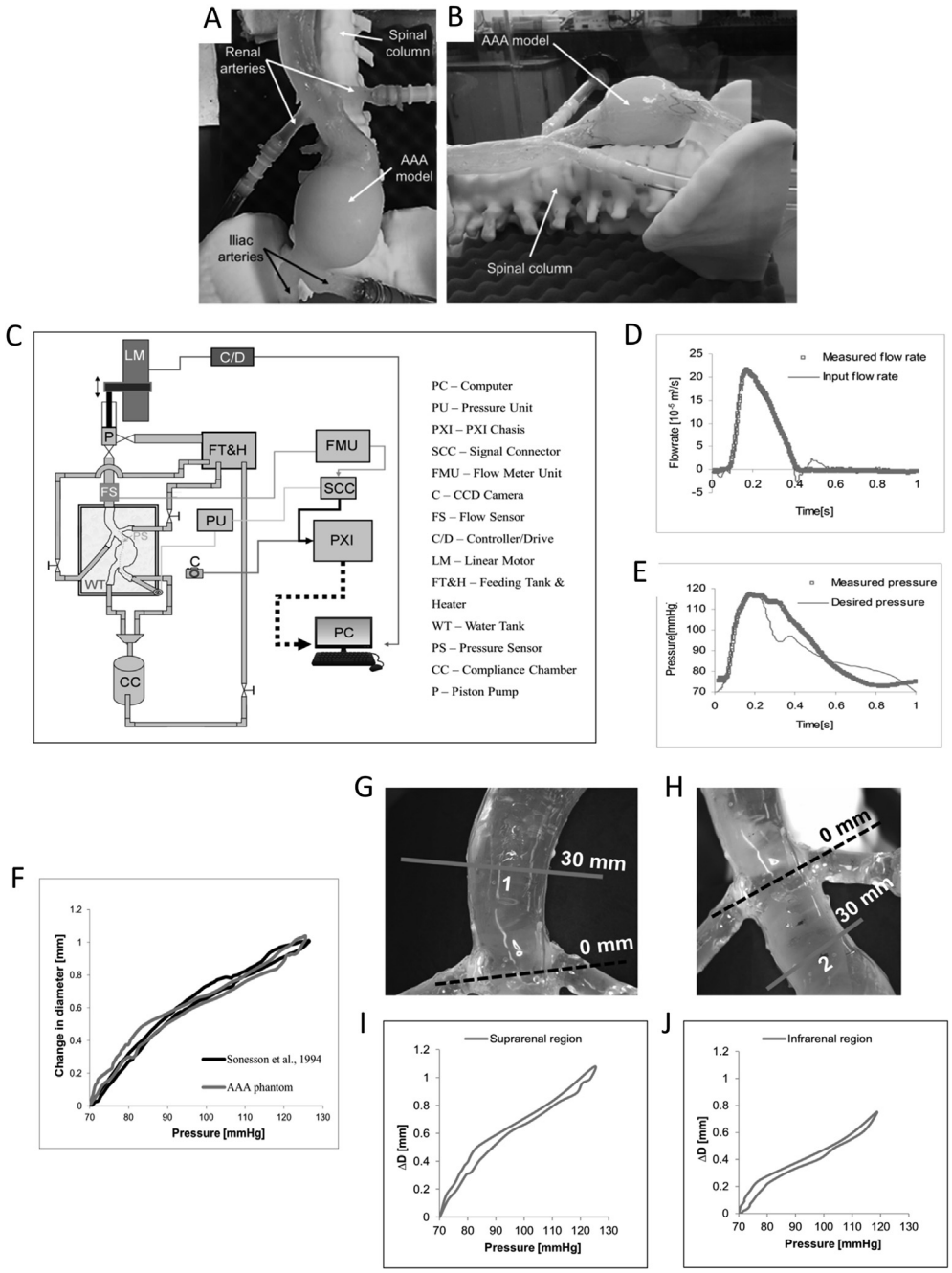

Figure 2. Patient-specific abdominal aortic aneurysm (AAA) silicone perfusion model mounted on a spinal column and flow simulator set-up. (A) Anterior view; (B) right view; (C) the schematic and components of the AAA flow simulator; (D) suprarenal flowrate waveform; (E) suprarenal pressure waveform; (F) comparison of suprarenal pressure—change in diameter (P—ΔD) curve of the AAA silicone perfusion model with the P—ΔD curve for older patients with AAAs (Sonesson et al.)[20]; (G) suprarenal section 30 mm above the renal branching area; (H) infrarenal section 30 mm below the renal branching area; (I) suprarenal P—ΔD curve; (J) infrarenal P—ΔD curve.

and common iliac arteries, was fabricated from translucent silicone elastomers by the injection moulding technique as previously described for idealised cases (Fig. 2A, B).[15,16] This perfusion model was based on a 72-year-old patient, with the three-dimensional (3D) geometry segmented within the commercially available image reconstruction software package Mimics 16.0 (Materialise, Leuven, Belgium). The AAA had a conical-shaped proximal neck with constant internal diameters of 23 mm (cranial) and 27 mm (caudal) on overall circumferences, neck length of 48 mm, and infrarenal neck angulation of 57°.

The maximum aneurysm outer diameter was 65 mm, iliac bifurcation inner diameter was 33 mm, and the left/right common iliac inner diameters were 13 mm. The arterial wall was replicated by Elastosil 4641 silicone (Wacker Chemie AG, Munich, Germany) with 5% silicone fluid (Dow Corning, UK) by weight and the ILT was replicated by Elastosil 4600 (Wacker Chemie AG, Germany) silicone with 25% silicone

Table 2. Outer diameter of the perfusion model infrarenal neck after device implantation at rest, without pressurisation; chronic outward and radial resistive force measurements, and calculated circumferential loading/unloading cycle energy loss at the infrarenal region; perfusion model abdominal aortic aneurysm (AAA) compliance; pulse wave velocity (PWV); reflection coefficient (Γ); and pulsatile arterial energy loss (PAEL) parameter comparisons for unstented/stented sections within the supra/infrarenal perfusion model's regions, at the 95% Mann–Whitney confidence interval (CI).

Device	Neck outer diameter after device implantation (mm)	Chronic outward force (N/cm)	Radial resistive force (N/cm)	Energy loss (hysteresis) (mm/mmHg)	PAEL Median (IQR) (mm/mmHg)	CI (% variation)[a]	*p*
Unstented	28.00	NA	NA	NA	2.3 (2.1–2.5)	NA	NA
MFM	28.14	0.06	0.84	0.03	3.3 (3.0–3.4)	(48.5–33.3)	<.001
EndurantII	28.63	0.54	2.85	0.15	2.3 (2.0–2.5)	(−9.4 to 7.6)	.903
Excluder	28.49	0.34	1.70	0.05	2.3 (2.0–2.4)	(54.7–40.5)	<.001
Zenith	28.31	0.67	2.88	0.14	2.7 (2.6–2.9)	(27.1–10.2)	<.001
Fortron	28.24	0.03	0.11	0.01	2.6 (2.3–2.9)	(23.1–3.6)	.006

	Perfusion AAA model wall compliance						PWV			Γ		
	Suprarenal Median (IQR) (10^{-4}/mmHg)	CI (% variation)[a]	*p*	Infrarenal Median (IQR) (10^{-4}/mmHg)	CI (% variation)[a]	*p*	Median (IQR) (m/s)	CI (% variation)[a]	*p*	Median (IQR) (%)	CI (% variation)[a]	*p*
Unstented	7.1 (6.9–7.6)	NA	NA	5.4 (5.2–5.7)	NA	NA	10.6 (10.4–11.0)	NA	NA	7.6 (7.4–7.8)	NA	NA
EndurantII	5.1 (5.0–6.1)	(−16.4 to −27.9)	<.001	4.8 (4.2–5.0)	(−12.4 to −22.4)	<.001	15.1 (14.2–15.2)	(43.5–39.5)	<.001	23.7 (23.4–24.0)	(212.6–207.8)	<.001
MFM	6.4 (5.8–7.3)	(−5.0 to −17.8)	.002	5.4 (4.8–6.2)	(−7.4 to +8.8)	.925	10.9 (10.5–11.0)	(−3.4 to 0.4)	.164	8.2 (8.0–8.4)	(11.0–5.7)	<.001
Excluder	6.9 (6.2–7.7)	(−8.8 to 3.8)	.675	4.9 (4.4–4.9)	(−9.7 to −17.5)	<.001	14.9 (14.6–15.0)	(41.4–37.4)	<.001	23.2 (22.9–23.5)	(206.4–201.2)	<.001
Zenith	6.0 (5.7–6.7)	(−10.0 to −19.2)	<.001	5.3 (4.4–5.8)	(−2.6 to 14.0)	.262	11.1 (10.9–11.4)	(6.5–2.7)	<.001	8.9 (8.8–9.3)	(20.9–15.8)	<.001
Fortron	6.1 (5.7–6.8)	(−8.4 to −18.5)	<.001	5.2 (5.0–5.6)	(−0.15 to +8.3)	.057	10.8 (10.6–11.1)	(3.8–0.3)	.036	8.6 (8.3–8.8)	(15.5–11.0)	<.001

Note. IQR = interquartile range; NA = not applicable.

[a] A negative sign refers to a percentage decrease; other values refer to percentage increase.

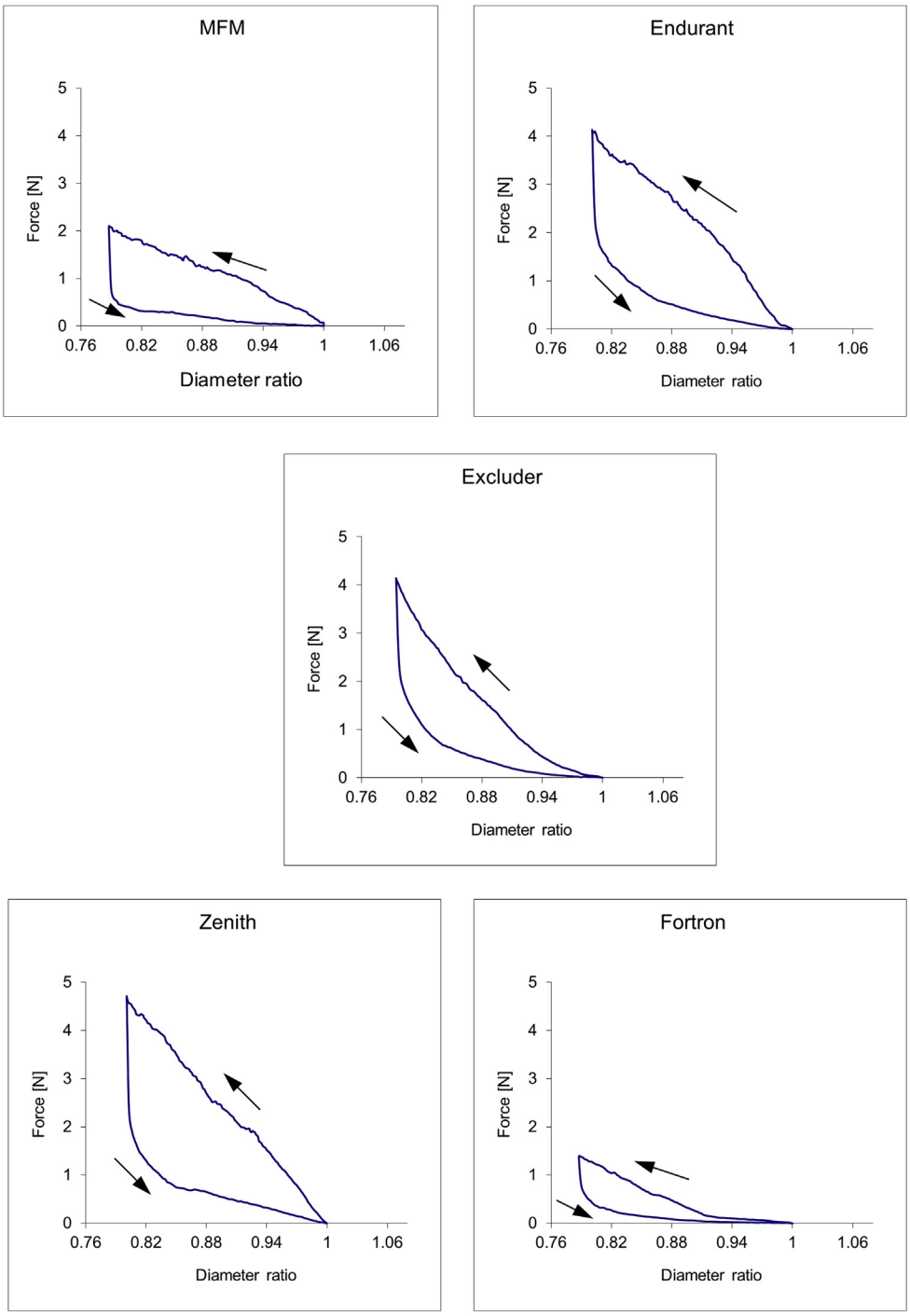

Figure 3. Deformation characteristics of all five devices during the circumferential loading (radial resistive) and unloading (chronic outward) cycles.

fluid (Dow Corning, Barry, UK) by weight. Owing to poor resolution of the computed tomography images the aortic wall thickness could not be measured and reconstructed. Therefore, the aortic wall thickness was assumed to be constant at 2 mm. The Young's Modulus for the silicone wall and ILT was 1.2 and 0.2 MPa, respectively, as tested on a uniaxial tensile testing machine (Instron 5544). These elastic properties were within previously reported tensile testing values for the abdominal aortic wall (1—6 MPa)[17] and ILT (0.05—0.27 MPa)[18] tissues. The spinal column model (Fig. 2A, B) was rapid prototyped by a 3D printer (Stratasys Prodigy Plus; Stratasys, Eden Prairie, MN, USA) and supported the AAA model.

Flow simulator system

Blood was replicated with 56% deionised water and 44% glycerine (Univar Ltd, West Yorkshire, UK) that had a dynamic viscosity of 0.0035 Pa•s at 37 °C, as found from a digital cone and plate viscometer (DV-II +PRO; Brookfield Engineering,

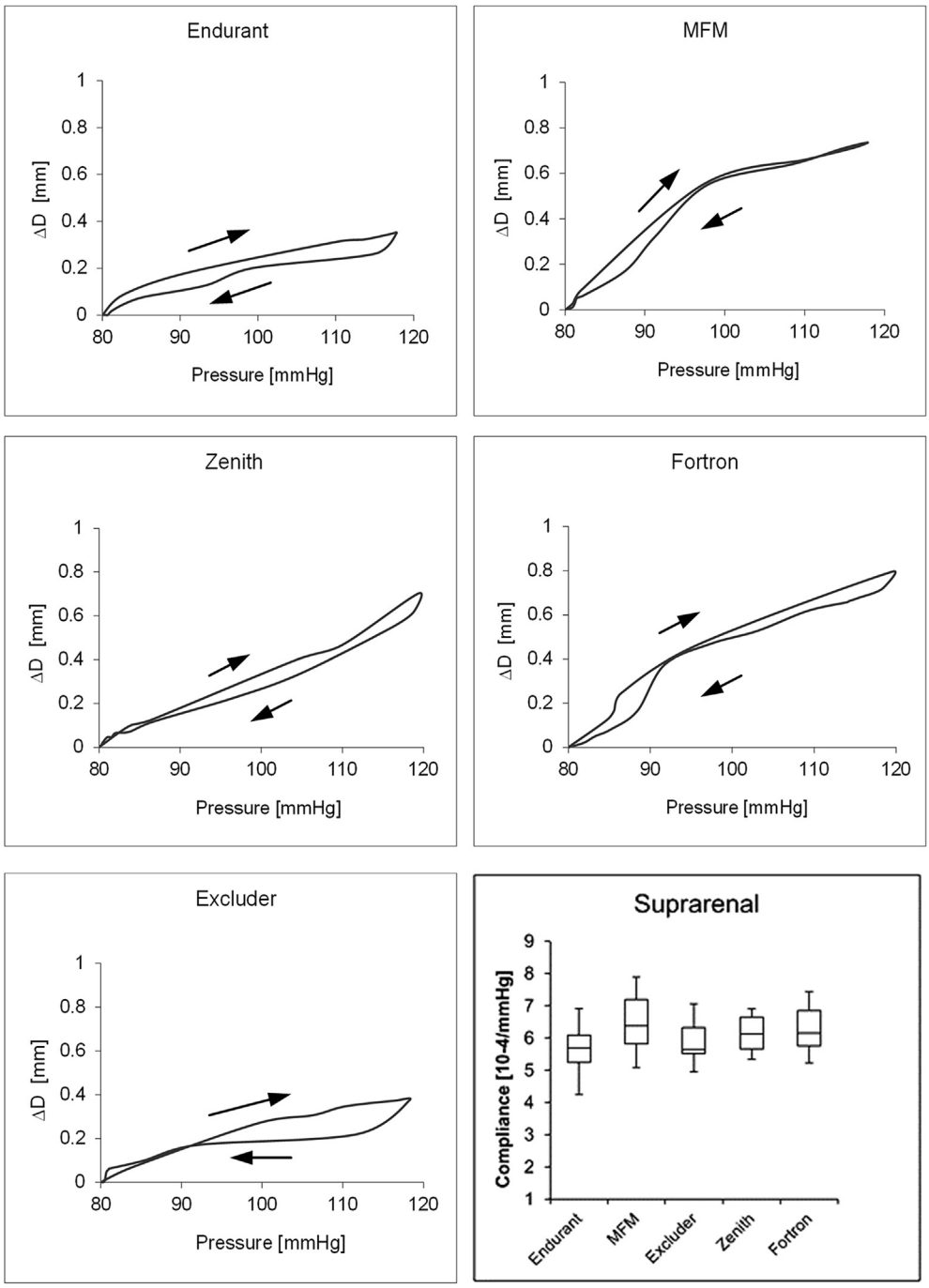

Figure 4. Pressure—change in diameter (P—ΔD) curves for the stented abdominal aortic aneurysm perfusion model at the suprarenal region (section 1) and box and whiskers plot of the arterial wall compliance. The centre line of the box denotes the median value, the extremes of the box represent the interquartile range, and the whiskers refer to the maximum and minimum data range.

Brookfield, WN, USA) and a density of 1,055 kg/m^3 found by a 50-mL burette and weighing scales. The required temperature of 37 °C was controlled by a heating unit (Julabo Ltd, Peterborough, UK), with constant fluid stirring.

A custom-built flow simulator replicated the aortic flowrate and pressure waveforms (Fig. 2C—E)[19] by a programmable linear actuator (Aerotech, Wythenshawe, UK). An ultrasonic flow meter (TS410 plug-in module; Transonic, Ithaca, NY, US) and flowsensor (25PXN Inline flow sensor; Transonic) recorded the flowrates. Twenty-two and 28% of the inlet flowrate travelled through each renal and common iliac arteries, respectively.[19] A distal compliance chamber and outlet valves controlled the pressure within physiological limits (Fig. 2C). The pressure waveform was recorded using a 3F pressure catheter (Scisense Inc., London, ON, Canada), positioned at the current site of measurement, along the imaginary centreline of each device. The average difference between the supracoeliac input (230 mL/s) and measured peak flowrate (220.8 mL/s), pressure (input 119 mmHg; output 114 mmHg) were <5%, as shown in Fig. 2(D, E).

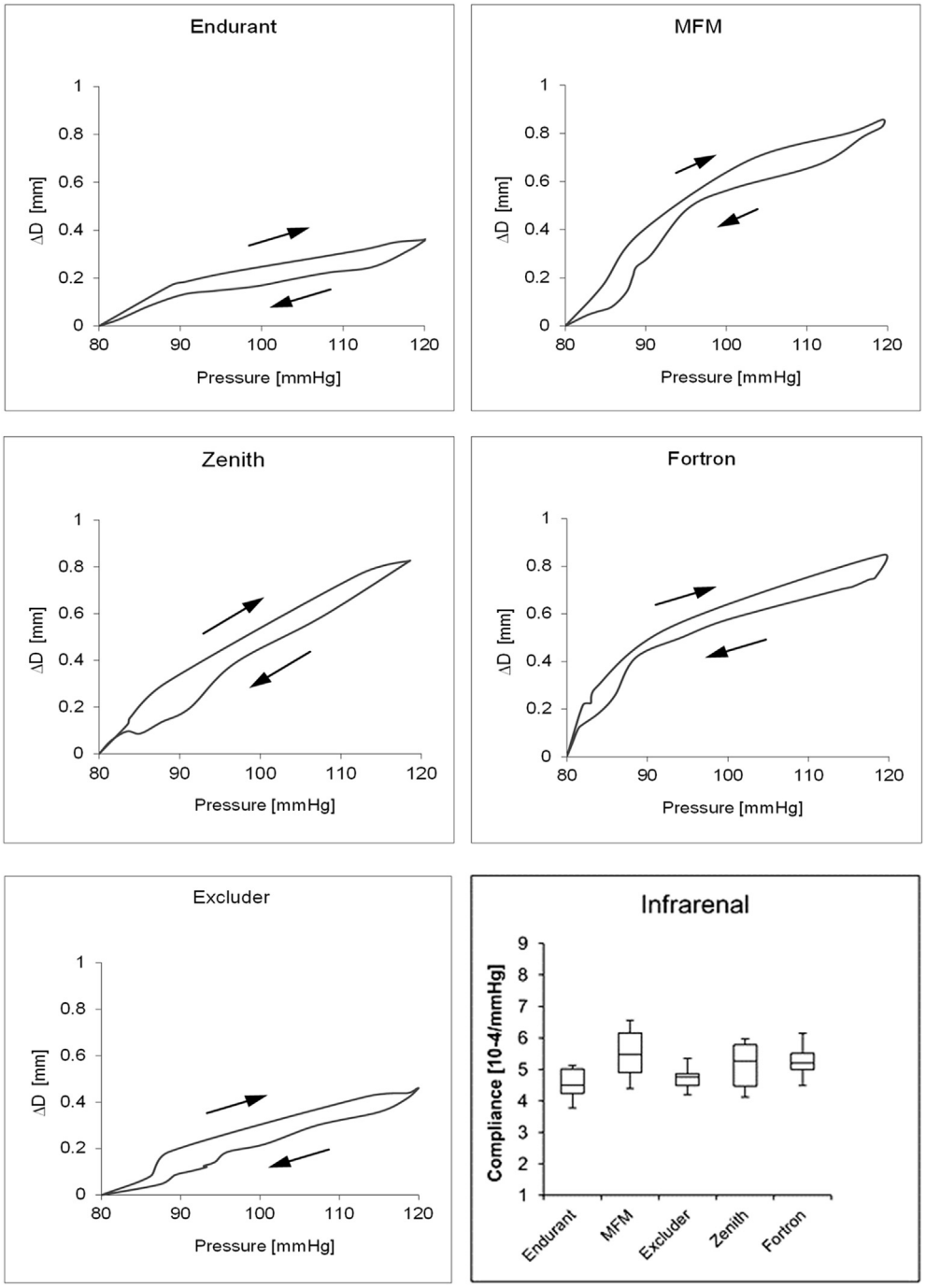

Figure 5. Pressure—change in diameter (P—ΔD) curves for the stented abdominal aortic aneurysm perfusion model at the infrarenal region (section 2) and box and whiskers plot of the arterial wall compliance. The centre line of the box denotes the median value, the extremes of the box represent the interquartile range, and the whiskers refer to the maximum and minimum data range.

The change in diameter (ΔD) was measured by a 4-mega pixel charge-coupled device camera (Dalsa 4M30; Dalsa Corp., Waterloo, ON, Canada) with attached Schneider Enlarger lens (aperture F 2.8) and a frame rate of 30 frames/s. An automatic edge detection tool (IMAQ software; National Instruments, Newbury, UK) identified the outer edges of the perfusion model. The ΔP—ΔD curve found by Sonesson et al. describing the infrarenal stiffness behaviour of the arterial wall in a 69-year-old age group was used to validate the reproducibility of the human aortic wall behaviour within the perfusion model (Fig. 2F).[20] Pressure and change in diameter (ΔP—ΔD) measurements were taken at the suprarenal and infrarenal locations, 30 mm above and below the renal arteries, prior to stenting (Fig. 2G, H). The ΔP—ΔD supra- and infrarenal curves for the perfusion model are shown in Fig. 2 (I, J).

There was very good agreement between the replicated perfusion model's behaviour with the *in vivo* AAAs.

The C of the unstented and stented perfusion models were calculated by the following formula[21]:

$$C = \frac{1}{A_{sys}} \cdot \frac{(A_{sys} - A_{dias})}{(P_{sys} - P_{dias})} \quad (2)$$

Where the pressure (P) and area (A) were based on the systole and diastole values of the cardiac cycle. The perfusion model had a median compliance variation of 5.4—7.1 $\times$ 10^{-4}/mmHg. These results agreed with the noninvasive ultrasonic C measurements for the native aorta found by Vorp et al. (5.1—19.0 $\times$ 10^{-4}/mmHg).[21]

All statistical comparisons were generated within Minitab 16.2.0 statistical software (Minitab, State College, PA, USA) by employing the Mann—Whitney nonparametric confidence interval (CI) testing method. All comparisons were conducted for 20 pulse cycles at the 95% CI.

In order to compare and validate the results with other studies from the literature, the following derived parameters were calculated: pulsatile arterial energy loss (PAEL), PWV, and wave reflection coefficient (Γ).

PAEL

The $\Delta P—\Delta D$ curve of the perfusion model exhibits a hysteresis effect similar to the *in vivo* measurements of Sonesson et al. and Stefanadis et al.[20,22] This area within the aortic loop represents the PAEL.[22] The calculated PAEL for the unstented perfusion model, at the suprarenal location, was 3.5 mm/mmHg. This was within the descending aortic range of 3.16 to 14.10 mm/mmHg[22]

PWV

The PWV was measured by monitoring the pressures and diameters at the systolic and diastolic phases. These data were used to estimate the local PWV by applying Equation (3),[23] as shown in Table 2 at the infrarenal location.

$$PWV = \sqrt{\frac{A}{\rho}\frac{\Delta P}{\Delta A}} \quad (3)$$

Where, A is the diastolic cross-sectional area, ΔA is the difference between systolic and diastolic areas, ΔP is the difference between systolic and diastolic pressures, and ρ is the density of the fluid.

Wave reflections

The wave reflections generated within the infrarenal perfusion model, before and after stenting, were computed by Equation (4) (Table 2).[19] This equation calculates the proportion of the pressure waveform being reflected, and is given by the reflection coefficient (Γ),

$$\Gamma = \frac{\frac{A_U}{c_U} - \frac{A_S}{c_S}}{\frac{A_U}{c_U} + \frac{A_S}{c_S}} \quad (4)$$

Where A_U is the cross-sectional area upstream from the proximal side; A_S is the cross-sectional area at the location of the proximal side, c_U is the PVW upstream from the proximal side, and c_S is the PVW at the location of the proximal side.

RESULTS

Device deformation characteristics

The curves describing circumferential loading cycles and device deformation behaviour are shown in Fig. 3. The length of the stent in contact with the strip divided the circumferential load (Table 2), which presents the magnitudes of the radial resistive and COFs expressed in N/cm, for all five devices at the diastolic diameter of the aorta perfusion model. The Zenith and EndurantII devices had the highest RRF (up to 3 N/cm), while the Fortron device had the lowest magnitude of 0.11 N/cm. In the second half of the cycle, the Zenith devices had the highest COF of up to 0.68 N/cm, while the Fortron and MFM had the lowest magnitude of 0.03 N/cm and 0.06 N/cm, respectively. The MFM had the greatest discrepancy of 14-fold between the COF and RRF.

Arterial wall/device interface compliance

Figs. 4 and 5 show the $\Delta P—\Delta D$ curves for the stented perfusion model at the supra- and infrarenal locations, respectively. Equation (2) was applied to find the C based on these $\Delta P—\Delta D$ curves, as shown in Figs. 4 and 5. Table 2 shows the median and interquartile range and the percentage median C variations when compared with the unstented C, based on the 95% Mann—Whitney CI test. At the suprarenal region, all devices, except the Excluder, significantly decreased the compliance by 10—21% ($p < .002$). At the infrarenal region, EndurantII and Excluder significantly decreased the compliance by 9—11% ($p < .001$), while the MFM, Zenith, and Fortron did not significantly ($p < .057$) influence C. At the infrarenal region, the MFM did not significantly alter PAEL (median 2.3 mmHg [$p = .903$]), while the other devices increased the PAEL by 13—44% ($p < .006$) (Table 2).

Stented perfusion model pulse wave analysis

The PWV of the unstented infrarenal section had a median value of 10.6 m/s, which was in agreement with the postoperative findings of Paraskevas et al.,[24] who, postoperatively, measured the mean aortic PWVs of 7.84 $\pm$ 1.85 m/s and 10.08 $\pm$ 1.57 m/s within AAA cases. The PWV ranged from 10.9 m/s (MFM, $p = .164$) to 15.1 m/s (EndurantII, $p < .001$) for all devices tested (see Table 2). High PWVs were recorded for the EndurantII (15.1 m/s; $p < .001$) and Excluder (14.9 m/s; $p < .001$) devices. The Zenith, Fortron, and MFM devices recorded the lowest PWV measurements, with values of 11.1 m/s ($p < .001$), 10.8 m/s ($p = .036$), and 10.9 m/s ($p = .164$), respectively.

For the unstented infrarenal perfusion model, Γ had a median value of 7.6%, owing to the tapering vessel and decreased compliance across the suprarenal and infrarenal regions. The Γ was increased by 205—212% ($p < .001$) for

the EndurantII and Excluder devices, and by 8—17% ($p < .001$) for the MFM, Fortron, and Zenith devices.

DISCUSSION

This study assessed the deformation characteristics and the influence on the radial arterial compliance of five devices for the treatment of AAAs, within a patient-specific perfusion model.

The AAA model had an infrarenal neck angle of 57°, which falls within the IFU recommendations for four devices (not the MFM). The Zenith, Excluder, and Fortron devices can be used if the minimum neck length is 15 mm and the infrarenal neck angle is $<60°$, while the EndurantII can be used if the infrarenal neck angle is $<75°$, for the same minimum neck length of 15 mm. The IFU of the MFM do not specify a threshold for the infrarenal neck angulation. The different device lengths were a result of limited access to a wider range of devices, but they did comply with the IFU and did not alter the measurements. There was a maximum of 7% variation in the maximum proximal diameter between the devices (Table 1), which was unavoidable as the preferred intended for use aortic diameters, as documented by the manufacturers, were within the aorta's infrarenal diameter range.

Increased pulse wave velocity[25] and low radial force can affect stent fixation leading to migration,[26] while a high radial force promotes continued dilation leading to migration, Type I endoleak.[27] Previous studies applied point loads on stents to assess the radial force.[28] The problem with this method is that stents do not experience point loads *in vivo*. Another approach has externally compressed stent/devices,[29] and this study found the stents/SGs to deform asymmetrically with hysteresis during the loading and unloading cycles. Johnston et al. concluded that no usable relationship between pressure and area reduction could be determined as a result of this asymmetrical deformation.[29] We applied an axisymmetric loading. The advantage of this approach is the realistic response of the stent, which provides quantifiable results.[29] Duda et al. obtained the radial resistive and chronic outward circumferential forces for four 8-mm diameter uncovered self-expanding stents,[14] observing similar behaviour during loading/unloading, as was found in this study (Fig. 3).

The Excluder and EndurantII devices significantly decreased C when compared with the unstented perfusion model, as it can be seen in Fig. 5 and Table 2. This resulted in a decreased compliance of 18—23% and 14—25% for the suprarenal and infrarenal regions, respectively. MFM, Zenith, and Fortron had a reduced compliance of 11—14% and 1—7% for the suprarenal and infrarenal regions, respectively. These differences in compliance between devices may not be associated with the different elastic properties of the fabrics. Although the measured compliance of Dacron (woven polyester) and expanded polytetrafluoroethylene (ePTFE) grafts, used for vascular reconstruction,[30] showed that the Dacron has a higher compliance value ($1.8 \pm 1.2\%$ per mmHg $\times 10^{-2}$) than ePTFE ($1.2 \pm 0.3\%$ per mmHg $\times 10^{-2}$), these materials come with different textile structure of the woven design in an endograft, which may affect their behaviour. Moreover, the diameter of the woven polyester for EndurantII and ePTFE for Excluder is in a relaxed state, when the oversized device is stressed in the arterial wall.

The PAEL within the infrarenal region was increased by the presence of the devices (Table 2; Fig. 5). This increase in PAEL may result in decreased distal perfusion, increased pressure wave reflections, and increased pulsatile mechanical stress at the interface between the noncompliant stented vessels and the native artery.[5,6] The elasticity of the arterial wall is responsible for the existence of wave reflections. The propagating pressure or flow waveforms will be reflected if the wave encounters any change in calibre along the arterial wall, such as a variation in cross-sectional area or material properties as given by Equation (4).[19] This variation in arterial calibre occurred after the insertion for all five devices, with varying degrees of severity. The early arrival of a reflected wave increases left ventricular load, which affects both ventricular emptying and driving pressure for coronary perfusion,[19,31] which eventually leads to low cardiac output, impaired coronary perfusion, heart failure, hypertension, and shock.[19,32] The Γ measurements that offer superiority to one device over another may characterise the situations of highly angulated AAA necks, as it is the case in this study, which has not yet been reported. Therefore, caution should be taken when interpreting these results.

This study found differences between the devices' performance. These differences arise mainly from the unique combination of material properties for the fabric and stent in each device (Table 1), and partly from the stent struts configurations. Three devices have a Z stent design (EndurantII, Zenith, and Excluder), one device has a proximal diamond stent design (Fortron), and one device has a braided mesh design (MFM). The stent design of the latter two devices produced the smallest radial forces among all tested devices as showed in Table 2. This fact may suggest that similar stent designs may be suitable towards achieving the right balance for future devices, between compliant device behaviour and fixation radial force, which would prevent proximal migration without stiffening the arterial wall.

The patient-specific perfusion model was chosen to recreate, as closely as possible, an example of real-life geometrical constraints, in which the devices have to perform. The ILT did not affect the compliance measurements, but it was replicated as part of a complex perfusion model. Part of the aim of this study was to predict how these devices may behave in real patients. Further studies may be carried out regarding the influence of anatomy over the device performance, where straight cylindrical models can be used for performance comparison.

Study limitations

Two limitations to the circumferential loading test approach are the unknown friction effects and local impingement of

the stent against the roller and base. With the circumferential loaded test, employing a combination of two rollers eliminated the local impingement effects. The film used, Tyvek (DuPont), has a low coefficient of friction.

We assumed a homogenous and isotropic silicone wall, which is in contact with the device wall, thus creating a composite material. That assumption allowed the use of Equation (2) for calculating wall compliance because the fabric of the SGs was not fully stretched after deployment, and the devices struts' strain within the ΔP was low. The relative movement between the stent struts and the aortic wall was not monitored. The PAEL parameter was assessed, only at the infrarenal neck, and not at the devices limbs, therefore it may not provide a strong relation with a potential cardiac risk.

CONCLUSION

The commercially available EVAR devices lower the arterial wall compliance at the stent/arterial wall interface after implantation. The Excluder device was found to be the most compliant in the suprarenal region, as this was the only tested device with no suprarenal fixation stent. The MFM was found to be the most compliant in the stented suprarenal region, while the Fortron device was the most compliant in the stented infrarenal region. From a clinical perspective, device selection based on minimum influence on the radial arterial compliance is advised, in order to prevent long-term device related complications. Future studies should analyse a wider range of commercially available devices to identify those that would pertain for low or zero complications rate.

CONFLICT OF INTEREST

None.

FUNDING

None.

APPENDIX A. SUPPLEMENTARY DATA

Supplementary data related to this article can be found at http://dx.doi.org/10.1016/j.ejvs.2015.07.041.

REFERENCES

1 Beebe HG, Cronenwett JL, Katzen BT, Brewster DC, Green RM. Vanguard Endograft Trial Investigators. Results of an aortic endograft trial: impact of device failure beyond 12 months. *J Vasc Surg* 2001;**33**:S55—63.
2 Morris L, Stefanov F, McGloughlin T. Stent graft performance in the treatment of abdominal aortic aneurysms: the influence of compliance and geometry. *J Biomech* 2013;**46**:383—95.
3 Bryce Y, Rogoff P, Romanelli D, Reichle R. Endovascular repair of abdominal aortic aneurysms: vascular anatomy, device selection, procedure, and procedure-specific complications. *Radiographics* 2015;**35**:593—615.
4 Humphery JD, Na S. Elastodynamics and arterial wall stress. *Ann Biomed Eng* 2002;**30**:509—23.
5 Tortoriello A, Pedrizzetti G. Flow-tissue interaction with compliance mismatch in a model stented artery. *J Biomech* 2004;**37**:1—11.
6 Back M, Kopchok G, Mueller M, Cavaye D, Donayre C, White RA. Changes in arterial wall compliance after endovascular stenting. *J Vasc Surg* 1994;**19**:905—11.
7 Vernhet H, Demaria R, Juan JM, Oliva-Lauraire MC, Sénac JP, Dauzat M. Changes in wall mechanics after endovascular stenting in the rabbit aorta: comparison of three stent designs. *Am J Roentgenol* 2001;**176**:803—7.
8 Ene F, Delassus P, Morris L. The influence of computational assumptions on analysing abdominal aortic aneurysm haemodynamics. *Proc Inst Mech Eng H* 2014;**228**:768—80.
9 Pihkala J, Thyagarajan GK, Taylor GP, Nykanen D, Benson LN. The effect of implantation of aortic stents on compliance and blood flow an experimental study in pigs. *Cardiol Young* 2001;**11**:173—81.
10 Brugaletta S, Gogas BD, Garcia-Garcia HM, Faroog V, Girasis C, Heo JH, et al. Vascular compliance change of the coronary vessel wall after bioresorbable vascular scaffold implantation in the treated and adjacent segments. *Circ J* 2012;**76**:1616—23.
11 Cheng CP, Parker D, Taylor CA. Quantification of wall shear stress in large blood vessels using Lagrangian interpolation functions with cine phase-contrast magnetic resonance imaging. *Ann Biomed Eng* 2002;**30**:1020—32.
12 Vlachopoulos C, Aznaouridis K, Stefanadis C. Prediction of cardiovascular events and all-cause mortality with arterial stiffness: a systematic review and meta-analysis. *J Am Coll Cardiol* 2010;**55**:1318—27.
13 Duerig TW, Pelton AR, Stoeckel D. The utility of superelasticity in medicine. *Biomed Mater Eng* 1996;**6**(4):255—66.
14 Duda SH, Wiskirchen J, Tepe G, Blitzer M, Kaulich TW, Stoeckel D, et al. Physical properties of endovascular stents: an experimental comparison. *J Vasc Interv Radiol* 2000;**11**:645—54.
15 Ene F, Gachon C, Delassus P, Carroll R, Stefanov F, O'Flynn P, et al. In vitro evaluation of the effects of intraluminal thrombus on abdominal aortic aneurysm wall dynamics. *Med Eng Phys* 2011;**33**:957—66.
16 Morris L, O'Donnell P, Delassus P, McGloughlin T. Experimental assessment of stress patterns in abdominal aortic aneurysms using the photoelastic method. *Strain* 2004;**40**:165—72.
17 Raghavan ML, Webster MW, Vorp DA. Ex vivo biomechanical behavior of abdominal aortic aneurysm: assessment using a new mathematical model. *Ann Biomed Eng* 1996;**24**:573—82.
18 Wang DH, Makaroun M, Webster MW, Vorp DA. Mechanical properties and microstructure of intraluminal thrombus from abdominal aortic aneurysm. *J Biomech Eng* 2001;**123**:536—9.
19 Nichols WW, O'Rourke MF. *McDonald's blood flow in arteries: theoretical, experimental and clinical principles*. Chapter 9: Contours of pressure and flow waves in arteries. 5th edn. London: Hodder Arnold; 2005. p. 165—91.
20 Sonesson B, Länne T, Vernersson E, Hansen F. Sex difference in the mechanical properties of the abdominal aorta in human beings. *J Vasc Surg* 1994;**20**:959—69.
21 Vorp DA, Mandarino WA, Webster MW, Gorcsan 3rd J. Potential influence of intraluminal thrombus on abdominal aortic aneurysm as assessed by a new non-invasive method. *Cardiovasc Surg* 1996;**4**:732—9.
22 Stefanadis C, Dernellis J, Vlachopoulos C, Tsioufis C, Tsiamis E, Toutouzas K, et al. Aortic function in arterial hypertension determined by pressure-diameter relation: effects of diltiazem. *Circulation* 1997;**96**:1853—8.
23 Wylie EB, Streeter VL. *Fluid transients*. New York: McGraw-Hill Book Co.; 1978.

24 Paraskevas KI, Bessias N, Psathas C, Akridas K, Nikitas G, Andrikopoulos V, et al. Evaluation of aortic stiffness (aortic pulse—wave velocity) before and after elective abdominal aortic aneurysm repair procedures: a pilot study. *Open Cardiovasc Med J* 2009;**3**:173—5.
25 Tzilalis VD, Kamvysis D, Panagou P, Kaskarelis I, Lazarides MK, Perdikides T, et al. Increased pulse wave velocity and arterial hypertension in young patients with thoracic aortic endografts. *Ann Vasc Surg* 2012;**26**:462—7.
26 Moore JE, Berry JL. Fluid and solid mechanical implications of vascular stenting. *Ann Biomed Eng* 2002;**30**:498—508.
27 Mattes J, Chemelli A, Wick M, Soimu D, Pontow C, Lopez A, et al. Evaluation of a new computerized analysis system developed for the processing of CT follow-up scans after EVR of infrarenal aneuysm. *Eur J Radiol* 2012;**81**:496—501.
28 Flueckiger F, Sternthal H, Klein GE, Aschauer M, Szolar D, Kleinhappl G. Strength, elasticity, and plasticity of expandable metal stents: in vitro studies with three types of stress. *J Vasc Interv Radiol* 1994;**5**:745—50.
29 Johnston CR, Lee K, Flewitt J, Moore R, Dobson GM, Thornton GM. The mechanical properties of endovascular stents: an in vitro assessment. *Cardiovasc Eng* 2010;**10**:128—35.
30 Tai NR, Salacinski HJ, Edwards A, Hamilton G, Seifalian AM. Compliance properties of conduits used in vascular reconstruction. *Br J Surg* 2000;**87**:1516—24.
31 Zannoli R, Schiereck P, Celletti F, Branzi A, Magnani B. Effects of wave reflection timing on left ventricular mechanics. *J Biomech* 1999;**32**:249—54.
32 Ikonomidis I, Lekakis J, Papadopoulos C, Triantafyllidi H, Paraskevaidis I, Georgoula G, et al. Incremental value of pulse wave velocity in the determination of coronary microcirculatory dysfunction in never-treated patients with essential hypertension. *Am J Hypertens* 2008;**21**:806—13.

Eur J Vasc Endovasc Surg (2016) 51, 55

COUP D'OEIL

Endovascular Treatment of Double Hepatic Arterial Aneurysm

K. Spanos *, **A.D. Giannoukas**
Department of Vascular Surgery, University Hospital of Larissa, Faculty of Medicine, School of Health Sciences, University of Thessaly, Larissa, Greece

A 62 year old male presented with atypical right subcostal pain. Abdominal ultrasound showed an intra-hepatic arterial aneurysm while CT angiography of aorta and branch arteries also detected an additional aneurysm at the mid-portion of hepatic artery (yellow arrows). Endovascular treatment was undertaken firstly with coil embolization of the feeding branch of the intra-hepatic aneurysm coming off the right branch of hepatic artery proper followed by placement of a 6 × 50 mm covered stent (Viabahn, Gore; red arrows) proximally. Completion angiography confirmed the exclusion of both aneurysms and the patient was discharged the next day on dual antiplatelet therapy (clopidogrel 75 mg, aspirin 100 mg).

* Corresponding author.
E-mail address: spanos.kon@gmail.com (K. Spanos).

http://dx.doi.org/10.1016/j.ejvs.2015.10.006